pH-Controlled Change of the Metal Coordination in a Dicopper(II) Complex of the Ligand H−BPMP: Crystal Structures, Magnetic Properties, and Catecholase Activity

S. Torelli, C. Belle,* I. Gautier-Luneau, and J. L. Pierre*

Laboratoire de Chimie Biomimétique (LEDSS, UMR CNRS 5616), Université J. Fourier, BP 53, 38041 Grenoble Cedex 9, France

E. Saint-Aman

Laboratoire d'Electrochimie Organique et de Photochimie Redox (UMR CNRS 5630), Université J. Fourier, BP 53, 38041 Grenoble Cedex 9, France

J. M. Latour, L. Le Pape, and D. Luneau

CEA-Grenoble, SCIB/DRFMC (UMR CNRS 5046), 17, rue des Martyrs, 38054 Grenoble Cedex 9, France

Received December 20, 1999

The dinucleating ligand 2,6-bis[(bis(2-pyridylmethyl)amino)methyl]-4-methylphenol (H−BPMP) has been used to synthesize the three dinuclear Cu(II) complexes $[Cu_2(BPMP)(OH)][ClO_4]_2 \cdot 0.5C_4H_8O$ (**1**), $[Cu_2(BPMP)(H_2O)_2](ClO_4)_3 \cdot 4H_2O$ (**2**), and $[Cu_2(H-BPMP)][(ClO_4)_4] \cdot 2CH_3CN$ (**3**). X-ray diffraction studies reveal that **1** is a μ-hydroxo, μ-phenoxo complex, **2** a diaqua, μ-phenoxo complex, and **3** a binuclear complex with Cu−Cu distances of 2.96, 4.32, and 6.92 Å, respectively. Magnetization measurements reveal that **1** is moderately antiferromagnetically coupled while **2** and **3** are essentially uncoupled. The electronic spectra in acetonitrile or in water solutions give results in accordance with the solid-state structures. **1** is EPR-silent, in agreement with the antiferromagnetic coupling between the two copper atoms. The X-band spectrum of powdered **2** is consistent with a tetragonally elongated square pyramid geometry around the Cu(II) ions, in accordance with the solid-state structure, while the spectrum in frozen solution suggests a change in the coordination geometry. The EPR spectra of **3** corroborate the solid-state and UV−visible studies. The ^{1}H NMR spectra also lead to observations in accordance with the conclusions from other spectroscopies. The electrochemical behavior of **1** and **2** in acetonitrile or in water solutions shows that the first reduction (Cu(II)Cu(II)−Cu(II)Cu(I) redox couple) is reversible and the second (formation of Cu(I)Cu(I)) irreversible. In water, **1** and **2** are reversibly interconverted upon acid/base titration (pK 4.95). In basic medium a new species, **4**, is reversibly formed (pK 12.0), identified as the bishydroxo complex. Only **1** exhibits catecholase activity (oxidation of 3,5-di-*tert*-butylcatechol to the corresponding quinone, $v_{max} = 1.1 \times 10^{-6}$ M^{-1} s^{-1} and $K_M = 1.49$ mM). The results indicate that the pH dependence of the catalytic abilities of the complexes is related to changes in the coordination sphere of the metal centers.

Introduction

Proteins containing dinuclear copper centers play paramount roles in biology, including dioxygen transport or activation, electron transfer, reduction of nitrogen oxides, and hydrolytic chemistry.[1] Among them many copper enzymes have oxidase or oxygenase activities. The structural aspects of the active sites dictate the type of activity.[2] Dinuclear Cu(II) complexes have received a great deal of attention.[1,3−6] They are of interest in the field of biomimetic chemistry to provide an improved understanding of the function of the biological sites and as potential catalysts for substrate oxidations. Binucleating ligands that contain a bridging phenoxo group have been widely used owing to their abilities to form stable complexes. One of the problems encountered in biomimetic inorganic chemistry is inherent in solution chemistry, particularly in the pH dependence of the coordination of the complexes. Herein, we describe the pH-induced changes in the coordination spheres of the dicopper(II) complex of the known ligand H−BPMP:[7,8] 2,6-bis[(bis(2-pyridylmethyl)amino)methyl]-4-methylphenol. Three complexes are described as well in solution as in the solid state. Their pH-driven interconversions and their redox properties have been studied. A fourth complex has been observed in solution (basic medium). One of the complexes exhibits catecholase activity.

* To whom correspondence should be addressed. E-mail: Jean-Louis.Pierre@ujf-grenoble.fr.

(1) Karlin, K. D.; Tyeklar, Z. *Bioinorganic Chemistry of Copper*; Chapman & Hill: New York, 1993.
(2) Solomon, E. I.; Sundaram, U. M.; Machonkin, T. E. *Chem. Rev.* **1996**, *96*, 2563−2605.
(3) Latour, J. M. *Bull. Soc. Chim. Fr.* **1988**, 508−523.
(4) Sorrell, T. N. *Tetrahedron* **1989**, *45*, 3−68.
(5) Vigato, P. A.; Tamburini, S.; Fenton, D. *Coord. Chem. Rev.* **1990**, *106*, 25−170.
(6) Kitajima, N. *Adv. Inorg. Chem.* **1992**, *39*, 1−77.
(7) Suzuki, M.; Kanatomi, H.; Murase, I. *Chem. Lett.* **1981**, 1745−1748.
(8) Borovik, A. S.; Papaefthymiou, V.; Taylor, L. F.; Anderson, O. P.; Que, L. *J. Am. Chem. Soc.* **1989**, *111*, 6183−6195.

10.1021/ic991450z CCC: $19.00
Published on Web 07/14/2000

Experimental Section

Commercial reagents (from Aldrich) were used as obtained without further purification. Solvents were purified by standard methods before use. Elemental analyses were performed by the CNRS Microanalysis Laboratory of Lyon, France.

Caution: Although no problems were encountered, suitable care and precautions should be taken when handling the perchlorate salts.

Spectrometry. Fast-atom bombardment (FAB) mass spectra in the positive mode were recorded on a Nermag R 1010C apparatus equipped with a M scan (Wallis) atom gun (8 kV, 20 mA). UV−visible spectra were obtained using a Perkin-Elmer Lambda 2 spectrophotometer operating in the range 200−900 nm with quartz cells. Temperature was maintained at 25 °C with the variable temperature unit. ϵ values are given in M^{-1} cm^{-1}. The deprotonation constants were determined in aqueous solutions (2.5×10^{-4} M); the ionic strength was adjusted with 0.01 M $NaClO_4$ in acidic medium. EPR spectra were recorded at 100 K on a BRUKER ESP 300E spectrometer operating at 9.4 GHz (X-band), with 3 mM solutions. Simulated spectra were calculated with a program written by F. Neese (Universität Konstanz, Germany, August 1994). ^{1}H NMR spectra were recorded on a BRUKER AC 200 spectrometer, at 25 °C, in D_2O with a little amount of DMSO as solvent. Chemical shifts (ppm) were referenced to solvent peaks. In D_2O, the pD was obtained from the measured pH-meter readings by adding 0.40 units.[9]

Magnetization Data. Magnetization experiments have been performed on a Quantum Design MPMS superconducting quantum interference device (SQUID) magnetometer operating at four magnetic fields 0.5, 1, 2.5, and 5 T over the temperature range 2−300 K. The powder samples (30−40 mg) were contained in a kel F bucket whose contribution was evaluated independently and subtracted from the sample data. The molar susceptibility corresponds to the resulting magnetization per magnetic field per mole ($[Cu_2(BPMP)(OH)][ClO_4]_2 \cdot 0.5C_4H_8O$ (**1**), 4.2×10^{-5} mol; $[Cu_2(BPMP)(H_2O)_2](ClO_4)_3 \cdot 4H_2O$ (**2**), 3.0×10^{-5} mol; $[Cu_2(H-BPMP)][(ClO_4)_4] \cdot 2CH_3CN$ (**3**), 3.6×10^{-5} mol). The diamagnetic contributions were estimated from Pascal's constants (**1**, -485×10^{-6} cm^3 mol^{-1}; **2**, -495×10^{-6} cm^3 mol^{-1}; and **3**, -530×10^{-6} cm^3 mol^{-1}.

Electrochemistry. Electrochemical experiments were carried out using a PAR model 273 potentiostat equipped with a Kipp-Zonen *xy* recorder. All experiments were run at room temperature under argon atmosphere. For analytical experiments, a standard three-electrode cell was used. For the experiments performed in acetonitrile as solvent, potentials are referred to an Ag/10 mM $AgNO_3$ reference electrode with 0.1 M tetra-*n*-butylammonium perchlorate (TBAP) as supporting electrolyte. Vitrous carbon disk electrodes for cyclic voltammetry (CV) (5 mm diameter) and rotating disk electrode (RDE) (3 mm diameter) were polished with 1 μm diamond paste. For the experiments performed in aqueous medium containing 0.1 M $NaClO_4$ as supporting electrolyte, the potentials were referenced to an SCE electrode.

X-ray Data Collection and Crystal Structure Determinations. The crystals of complexes **1** and **2** were mounted on a Enraf-Nonius CAD4 diffractometer using a graphite crystal monochromator (λ (Mo Kα) = 0.71073 Å) at 293 K. The reflections were corrected for Lorentz and polarization effects but not for absorption. The structures were solved by direct methods and refined using TEXSAN software.[10a]

a. Complex 1. $[Cu_2(C_{33}H_{33}ON_6)(OH)](ClO_4)_2 \cdot C_4H_8O$; $M_w = 944.77$, green block (0.2 mm × 0.2 mm × 0.1 mm), orthorhombic, space group $Pna2_1$, $a = 18.251(6)$ Å, $b = 16.795(3)$ Å, $c = 13.041(6)$ Å, $V = 3997(2)$ Å^3, $Z = 4$, Dx = 1.57 g cm^{-3}, $\mu = 1.265$ mm^{-1}. A total of 6426 reflections were collected in the range $4 \le 2\theta \le 60°$. All non-hydrogen atoms were refined with anisotropic thermal parameters. Hydrogen atoms were generated in idealized positions, riding on the carrier atoms, with isotropic thermal parameters except for the hydrogen atom of the hydroxyl group, which was localized on a difference Fourier map but not refined. Final cycle refinement, including 522 parameters, converged to $R(F) = 0.077$ and $R_w(F) = 0.064$ [for 2808, $F > 1\sigma(F)$] [$s = 1.61$, $(\Delta/\sigma)_{max} = 0.1$, $\Delta\rho_{max} = 0.75$ e Å^{-3}, $\Delta\rho_{min} = -0.62$ e Å^{-3}].

b. Complex 2. $[Cu_2(C_{33}H_{33}ON_6)(H_2O)_2](ClO_4)_3 \cdot 4H_2O$; $M_w = 1063.20$, green-blue block (0.2 mm × 0.3 mm × 0.1 mm), orthorhombic, space group *Pbcn*, $a = 16.300(2)$ Å, $b = 16.501(3)$ Å, $c = 16.654(7)$ Å, $V = 4479(2)$ Å^3, $Z = 4$, Dx = 1.576 g cm^{-3}, $\mu = 1.209$ mm^{-1}. A total of 7195 reflections were collected in the range $6° \le 2\theta \le 60°$. The crystal structure reveals that the tricationic molecular entity possesses a 2-fold axis symmetry. So only a half molecular unit and 1.5 perchlorate anions have been defined. One perchlorate anion is in a general position. The other is close to the 2-fold axis so that the chlorine atom was refined with a site occupation factor (sof) of 0.5, two oxygen atoms with a sof of 0.5, and one oxygen atom with a sof of 1. All non-hydrogen atoms were refined with anisotropic thermal parameters. Hydrogen atoms were generated in idealized positions, riding on the carrier atoms, with isotropic thermal parameters. Final cycle refinement, including 300 parameters, converged to $R(F) = 0.053$ and $R_w(F) = 0.073$ [for 2496, $F > 3\sigma(F)$] [$s = 2.73$, $(\Delta/\sigma)_{max} = 0.04$, $\Delta\rho_{max} = 0.49$ e Å^{-3}, $\Delta\rho_{min} = -0.33$ e Å^{-3}].

c. Complex 3. To avoid decomposition by loss of solvent, the crystal was glued in grease and the data were collected at a low temperature of 193 K for 5 h on a blue block crystal of dimensions 0.2 mm × 0.2 mm × 0.1 mm using the SIEMENS SMART CCD area detector diffractometer system equipped with a normal focus molybdenum-target tube operating at 2 kW (50 kV, 40 mA). The data were processed through the SAINT data reduction and SADABS softwares.[10b]

$[Cu_2(C_{33}H_{34}ON_6)(CH_3CN)_3(ClO_4)][Cu_2(C_{33}H_{34}ON_6)(CH_3CN)_2(C_4H_8O)(ClO_4)](ClO_4)_6 \cdot 1.5CH_3CN \cdot C_4H_8O$; $M_w = 2544.19$, triclinic, space group $P\bar{1}$, $a = 13.784(1)$ Å, $b = 15.684(1)$Å, $c = 24.701(1)$ Å, $\alpha = 88.860(1)°$, $\beta = 86.954(1)°$, $\gamma = 85.966(1)°$, $V = 5318.4(2)$ Å^3, $Z = 2$, Dx = 1.575 g cm^{-3}, $\mu = 1.081$ mm^{-1}. A total of 21 665 reflections were collected. The structure was solved using an automatic Patterson procedure and refined using TEXSAN software.[10a] All non-hydrogen atoms were refined with anisotropic thermal parameters. Hydrogen atoms were generated in idealized positions and refined, riding on the carrier atoms, with isotropic thermal parameters [$U(H) = 1.2U_{eq}(C)$ for aromatic hydrogen and $U(H) = 1.5U_{eq}(C)$ for nonaromatic hydrogen. One acetonitrile ligand is disordered on two sites with site occupation factors equal to 0.65 for C73 and C74 and 0.35 for C73* and C74*. Final cycle refinement including 1418 parameters converged to $R(F) = 0.058$ (for 9592, $F > 3\sigma(F)$), $R_w(F) = 0.066$ and goodness of fit $s = 2.05$ [$(\Delta/\sigma)_{max} = 0.05$, $\Delta\rho_{max} = 1.08$ e Å^{-3}, $\Delta\rho_{min} = -1.08$ e Å^{-3}].

Syntheses. The ligand H−BPMP was synthesized according to the preparation previously described[7,8] with some modifications. Under a dinitrogen atmosphere, a mixture of bis(2-pyridylmethyl)amine (2.90 g, 14.6 mmol) and triethylamine (3.03 g, 30 mmol) in 7 mL of dry THF was added dropwise to a stirred solution of 2,6-bis(chloromethyl)-4-methylphenol (1.5 g, 7.31 mmol) in 15 mL of dry THF at 0 °C. When the addition was completed, the resulting mixture was allowed to warm to room temperature. After 2.5 days, the resulting mixture was filtered and the filtrate was concentrated under reduced pressure. The residue was dissolved in 100 mL of methylene chloride, washed with brine, and dried over anhydrous Na_2SO_4. The solution was evaporated to dryness at reduced pressure, and a crude product was obtained as a sticky solid. Recrystallization from hexane/ether (1/1) afforded 3.30 g (86%) of pure H−BPMP as a whitish solid; mp 95 °C. Anal. Calcd for $C_{33}H_{34}N_6O_1$: C, 73.60; H, 6.46; N, 15.84. Found: C, 73.50; H, 6.49; N, 15.76.

a. Complex 1. $[Cu_2(BPMP)(OH)][ClO_4]_2 \cdot 0.5C_4H_8O$. To 300 mg (0.56 mmol) of H−BPMP dissolved in CH_3CN (10 mL), a solution of 427 mg of $Cu(ClO_4)_2 \cdot 6H_2O$ (1.12 mmol) in CH_3CN (5 mL) was added dropwise. The initial yellow solution turned dark-blue and was stirred for 10 min at room temperature. Then 160 μL (1.12 mmol) of Et_3N was added and the solution, which turned dark-green, was stirred for 30 min at room temperature. The solvent was partially removed under reduced pressure, and the resulting solution (10 mL) was allowed to stand overnight at −20 °C. A quantity of 395 mg of a green powder was collected by filtration (81%). Crystals of X-ray quality were obtained by vapor diffusion of THF in an CH_3CN solution of **1**. Anal. Calcd for $C_{33}H_{34}N_6O_{10}Cu_2Cl_2.0.5C_4H_8O$: C, 46.26; H, 4.22; N, 9.25;

(9) Glasoe, P. K.; Long, F. A. *J. Phys. Chem.* **1960**, *64*, 188.
(10) (a) *TEXSAN. Single-Crystal structure Analysis Software*, version 1.7; Molecular Structure Corporation: The Woodlands, TX, 1995. (b) *SADABS*, *SAINT*, version 4.050; Siemens Analytical X-ray Instruments: Madison, WI, 1992−1995.

Cu, 13.99; Cl, 7.80. Found: C, 46.00; H, 4.27; N, 8.91; Cu, 13.81; Cl, 7.33. UV−vis in CH_3CN: λ_{max} = 410 nm (ϵ = 480), 785 nm (ϵ = 280). FAB-MS (Matrix NBA) *m/e* = 656 $[(BPMP)(Cu)_2]^+$

b. Complex 2. $[Cu_2(BPMP)(H_2O)_2][(ClO_4)_3]\cdot 4H_2O$. An amount of 153 mg (0.29 mmol) of H−BPMP, distilled water (5 mL), and acetone (5 mL) were combined. The solution was stirred until complete solubilization (1 h), and 251 mg of $Cu(ClO_4)_2\cdot 6H_2O$ (0.635 mmol) in water (5 mL) was added dropwise. The solution turned brown instantaneously and was stirred for 3 h at room temperature. An amount of 5 mL of diethyl ether was added, and the solution was allowed to stand at 4 °C for 12 h. A green powder was recovered (294 mg, 65%). It was recrystallized by solubilization in water followed by slow evaporation of the solvent. Anal. Calcd for $C_{33}H_{37}N_6O_{15}Cu_2Cl_3\cdot 4H_2O$: C, 37.30; H, 4.27; N, 7.90; Cu, 11.95; Cl, 10.00. Found: C, 38.30; H, 4.12; N, 7.75; Cu,11.33; Cl, 10.06. UV−vis in H_2O: λ_{max} = 460 nm (ϵ = 710), 700 nm (ϵ = 180). FAB-MS (Matrix NBA) *m/e* = 855 $[(BPMP)(Cu)_2(ClO_4)_2 + 1H]^+$, 657 $[(BPMP)(Cu)_2 + 1H]^+$.

c. Complex 3. $[Cu_2(H-BPMP)][(ClO_4)_4]\cdot 2CH_3CN$. To 300 mg (0.56 mmol) of H−BPMP dissolved in CH_3CN (10 mL) a solution of 470 mg of $Cu(ClO_4)_2\cdot 6H_2O$ (1.26 mmol) in CH_3CN (5 mL) was added dropwise. The initial yellow solution turned dark-blue and was stirred for 10 min at room temperature. The solvent was partially removed under reduced pressure, and a few drops of diethyl ether were added. The resulting solution (10 mL) was allowed to stand for 3 days at −20 °C. An amount of 600 mg of a blue powder was collected by filtration (yield: 87%). Crystals of X-ray quality were obtained by vapor diffusion of THF in a solution of **3** in CH_3CN. Anal. Calcd for $C_{33}H_{34}N_6O_{17}Cu_2Cl_4\cdot 2CH_3CN$: C, 38.90; H, 3.77; N, 9.04; Cu, 11.9; Cl, 13.13. Found: C, 37.37; H, 4.07; N, 8.14; Cu, 10.25; Cl, 11.96. UV−vis in CH_3CN: λ_{max} = 610 nm (ϵ = 266). FAB-MS (Matrix NBA) *m/e* = 855 $[(BPMP)(Cu)_2(ClO_4)_2 + 1H]^+$, 756 $[(BPMP)(Cu)_2(ClO_4) + 1H]^+$, 657 $[(BPMP)(Cu)_2 + 1H]^+$

Catecholase Activities. The catecholase activity has been evaluated at 25 °C temperature by the reaction of the complexes with 3,5-di-*tert*-butylcatechol (3,5-DTBC). The absorption at λ_{max} = 410 nm (ϵ = 1900), characteristic of the formed quinone, was measured as a function of time. A 2.5×10^{-4} M solution of the complex with 100 equiv of 3,5-DTBC has been used, and the solution was saturated with 1 atm of dioxygen. Under theses conditions, catechol was not oxidized without copper complexes. For **1**, the same result was obtained in CH_3CN or in a mixture (CH_3CN/H_2O, 20/80) buffered at pH = 7. For **2** and **4**, measurements were performed in a mixture (CH_3CN/H_2O, 20/80). Under these conditions, no changes were observed from the initial solutions of complexes (UV−visible spectrophotometry). The pH was adjusted with $HClO_4$ or NaOH (1 M). The kinetic parameters were determined for 4.5×10^{-5} M solutions of **1** and 0.225− 0.45 mM solutions of the substrate.

Results

Description of Crystal Structures. a. Complex 1. The μ-hydroxo complex **1** had been previously structurally characterized.[11d] Nevertheless, a different crystalline form (crystal system and space group) has been obtained in the present study. This prompts us to detail its molecular structure. One molecule of THF solvent per complex entity crystallizes in the cell, increasing its volume, but the density is quite equivalent. An ORTEP view of dicationic complex **1** $[Cu_2(BPMP)(OH)]^{2+}$ is shown in Figure 1, and selected bond lengths and angles are given in Table 1. The crystal structure reveals that the two copper atoms are doubly bridged by the phenoxo and a hydroxo group. The pentacoordination of Cu1 and Cu2 is achieved by the tertiary amine and two pyridine nitrogens that are cis to each other. The coordination polyhedrons of both copper atoms are best described by distorted trigonal bipyramids with atoms O1, N3, N4 and O1, N5, N6 forming the trigonal planes where Cu1 and Cu2 are respectively located at 0.167 and 0.132 Å toward the O2 atom. By use of the method of Muetterties and Galy,[12] the shape-determinating dihedral angles e_3 are 61.1° for Cu1 and 61.9° for Cu2, close to the value 53.1° expected for a trigonal bipyramid, whereas it is 0.0° in a tetragonal pyramid. The Cu−N distances are in the range 1.995(8)−2.19(1) Å. The Cu−O distances in the Cu_2O_2 unit are in the range 1.891(8)−2.039(7) Å and slightly more asymmetric than other similar μ-phenoxo, μ-hydroxo copper(II) dimers.[11a,13,14] The four atoms Cu1, Cu2, O1, and O2 are in the same plane with a maximal deviation from the least-squares plane of 0.014(6) Å. Accordingly, the angles in the Cu_2O_2 unit are relatively close, the phenoxo Cu1−O1−Cu2, the hydroxo Cu1−O2−Cu2, O1−Cu1−O2, and O1−Cu2−O2 angles are respectively 95.7(2)°, 102.1(3)°, 82.5(3)°, and 79.7(3)°, which lead to the shortest distance Cu1···Cu2 of 2.966(1) Å compared to those for similar structures [2.992(2) Å for the same ligand,[11a] 3.053(4) [13] and 3.082(3) Å[14] with other μ-phenoxo, μ-hydroxo copper(II)

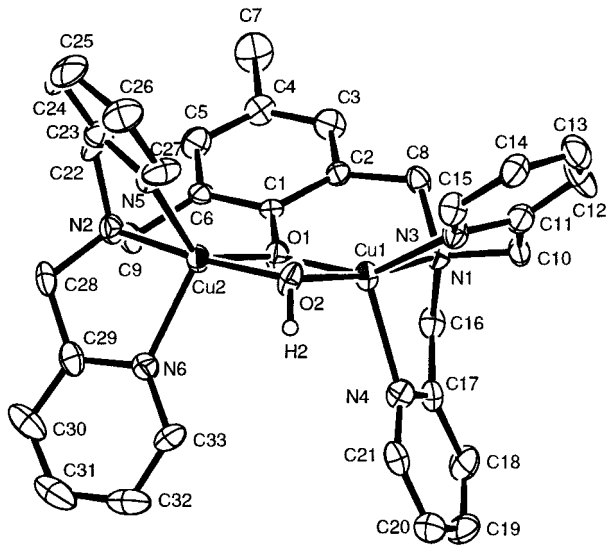

Figure 1. ORTEP plot of dicationic complex **1**. Hydrogens are omitted for clarity. Ellipsoids are drawn at the 30% probability level.

Table 1: Selected Distances (Å) and Bonds Angles (deg) for **1**

Cu1	Cu2	2.966(1)	Cu2	O2	1.922(8)
Cu1	O2	1.891(8)	Cu2	N2	1.995(8)
Cu1	O1	1.962(7)	Cu2	O1	2.039(7)
Cu1	N3	2.025(9)	Cu2	N5	2.038(8)
Cu1	N1	2.040(8)	Cu2	N6	2.094(9)
Cu1	N4	2.19(1)			

Cu1	O1	Cu2	95.7(2)	Cu1	O2	Cu2	102.1(3)
O2	Cu1	O1	82.5(3)	O2	Cu2	N2	171.8(3)
O2	Cu1	N3	98.7(3)	O2	Cu2	O1	79.7(3)
O2	Cu1	N1	169.6(3)	O2	Cu2	N5	99.5(3)
O2	Cu1	N4	109.8(3)	O2	Cu2	N6	103.2(3)
O1	Cu1	N3	148.3(3)	N2	Cu2	O1	93.4(3)
O1	Cu1	N1	90.0(3)	N2	Cu2	N5	82.4(3)
O1	Cu1	N4	103.7(3)	N2	Cu2	N6	82.8(3)
N3	Cu1	N1	84.0(3)	O1	Cu2	N5	136.1(3)
N3	Cu1	N4	105.6(3)	O1	Cu2	N6	105.2(3)
N1	Cu1	N4	78.9(3)	N5	Cu2	N6	117.4(4)

(11) (a) Holz, R. C.; Brink, J. M. *Inorg. Chem.* **1994**, *33*, 4609−4610. (b) Holz, R. C.; Brink, J. M.; Rose, R. A. *J. Magn. Reson., Ser. A* **1996**, *119*, 125−128. (c) Holz, R. C.; Bennett, B.; Chen, G.; Ming, L.-J. *J. Am. Chem. Soc.* **1998**, *120*, 6329−6335. (d) Maloney, J. J.; Glogowski, M.; Rohrbach, D. F.; Urbach, F. L. *Inorg. Chim. Acta* **1987**, *127*, L33−L35. (e) Rose, R. A.; Brink, J. M.; Holz, R. C. *Inorg. Chem.* **1996**, *35*, 2878−2885.

(12) (a) Muetterties, E. L.; Guggenberger, L. J. *J. Am Chem. Soc.* **1974**, *96*, 1748−1756. (b) Galy, J.; Bonnet, J. J.; Anderson, S. *Acta Chem. Scand.* **1979**, *A33*, 383−389.

(13) Sorrell, T. N.; Jameson, D. L.; O'Connor, C. J. *Inorg. Chem.* **1984**, *23*, 190−195.

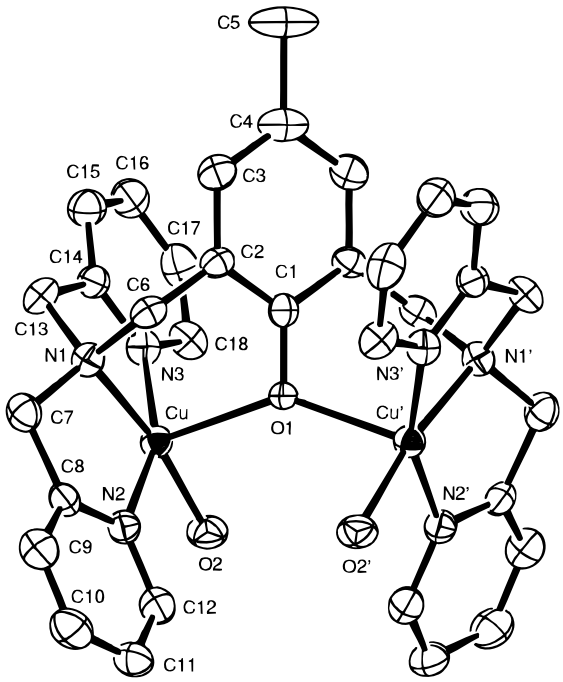

Figure 2. ORTEP plot of of tricationic complex **2**. Hydrogens are omitted for clarity. Ellipsoids are drawn at the 30% probability level.

Table 2: Selected Distances (Å) and Bonds Angles (deg) for **2**[a]

Cu	Cu′		4.139(1)	Cu	N1		2.027(4)
Cu	O1		2.189(2)	Cu	N2		1.993(4)
Cu	O2		2.005(4)	Cu	N3		2.000(4)
Cu	O1	Cu′	142.0(2)	N3	Cu	N1	83.4(2)
N2	Cu	N3	159.5(2)	N3	Cu	O1	94.7(2)
N2	Cu	O2	93.3(2)	O2	Cu	N1	171.3(2)
N2	Cu	N1	82.8(2)	O2	Cu	O1	94.2(1)
N2	Cu	O1	101.4(1)	N1	Cu	O1	94.1(1)
N3	Cu	O2	98.2(2)				

[a] ′Symmetry: (′) $-x, +y, 0.5 - z$.

dimers]. The phenolate ring is both tilted to the O1−O2 axis and twisted with respect to the O1−Cu2−O2−Cu1 plane. The tilting is seen by measuring the angle O2−O1−C1 (151.7(5)°) and the twisting from the torsion angles Cu1−O1−C1−C2 and Cu2−O1−C1−C6 (respectively, 9(1)° and −37(1)°). So Cu1, Cu2, and O2 lie on the same side of the plane (O1, C1, C2, C3, C4, C5, C6). The spatial disposition of the pyridine groups relative to each other around the copper atoms makes the metal site easily accessible (see another drawing of **1** and a stereoview (Figures S1-1 and S1-2) in the Supporting Information).

b. Complex 2. An ORTEP view of tricationic complex **2** $[Cu_2(C_{33}H_{33}ON_6)(H_2O)_2]^{3+}$ is shown in Figure 2 (a stereoview is given Figure S2-2 in Supporting Information), and selected bond lengths and angles are given in Table 2. The crystal structure reveals that the tricationic molecular entity possesses a 2-fold symmetry axis. So only half a molecular unit is crystallographically defined. The copper atom is bound by three nitrogen atoms from the tertiary amine and the two pyridines and by two oxygen atoms from the phenoxo bridge and a terminal water molecule. It is worth noting that in contrast to **1** the two pyridine groups are trans to each other in **2**. The pentacoordinated environment is described as a slightly distorted square pyramid whose apical position is occupied by the bridging phenoxo oxygen. The Muetterties−Galy[12] approach furnishes a shape-determinating dihedral angle $e_3 = 7.3°$ in this complex, in agreement with a slightly distorded square pyramid geometry. The square plane is defined by N1, N2, N3, and O2 atoms with a maximal deviation from the least-squares plane of 0.072(4) Å. The copper atom lies 0.21 Å out of the basal plane toward the apical O1 atom. The distances from copper to the equatorial atoms span the narrow range from 1.993(4) to 2.027(4) Å, and the apical Cu−O1 distance is the longest (2.189(2) Å). The Cu−O1−Cu′ bond angle is 142.0(2)°, while the phenolate ring is twisted relative to the Cu−O1−Cu′ plane with torsion angles Cu−O1−C1−C2 and Cu′−O1−C1−C2′ equal to 53.7(2)° (see another drawing of **2** in Figure S2-1 in the Supporting Information). Because of the 2-fold axis, copper atoms Cu and Cu′ are on different sides of the phenolate plane. The intermetallic distance Cu···Cu′ is 4.139(1) Å. It is the longest distance observed for a singly phenoxo-bridged dicopper(II) complex in which both coppers are in a tetragonal pyramidal environment with the distances 3.531, 3.726, 3.785, 4.09, and 4.128 Å.[15−19] This is due to the fact that the bridging phenoxo oxygen is apical to both copper atoms as in the last example.[19]

c. Complex 3. The structure consists of two crystallographically independent units $[Cu_2(C_{33}H_{34}ON_6)(CH_3CN)_3(ClO_4)]^{3+}$ and $[Cu_2(C_{33}H_{34}ON_6)(CH_3CN)_2(C_4H_8O)(ClO_4)]^{3+}$ that are different by the environment of one copper atom of each dinuclear complexes as seen in the ORTEP drawings in parts A and B of Figure 3. Selected bond lengths and angles are given in Table 3. In contrast to complexes **1** and **2** , the copper atoms (Cu1, Cu2) and (Cu3, Cu4) are not bridged by the phenol group, which is protonated and coordinated only to one copper atom. The coordination environment around Cu1 and Cu3 atoms are similar in octahedral geometry. Four nitrogen atoms (the tertiary amine, the two pyridine groups, and acetonitrile) form the square plane (where the mean-square deviations are 0.036 Å for (Cu1, N1, N2, N3, N7) and 0.026 Å for (Cu3, N10, N11, N12, N16)). The two oxygens from the phenol group and a perchlorate anion occupy axial positions. The Cu−N distances are in the range 1.983(5)−2.022(5) Å for Cu1 and 1.971(5)−2.033(4) Å for Cu2, while the Cu−O distances are longer because of the pseudo Jahn−Teller effect. The distances to the phenol oxygen are 2.432(4) Å for Cu1−O1 and 2.458(4) Å for Cu2−O2, showing the weaker donor character of protonated oxygen (compared to the distance of 2.240(6) Å [20] for the monodentate and unprotonated oxygen in the mononuclear copper(II) complex $[Cu(H_3L)(O_2CMe)]^+$). The copper atoms Cu2 and Cu4 noncoordinated to the phenol group are in square pyramidal environments. Cu2 and Cu4 are linked to nitrogen atoms of the tertiary amine, the pyridine groups, and solvent molecules; two acetonitrile molecules are coordinated to Cu2, while Cu4 is surrounded by one THF and one acetonitrile disordered on two sites. The Cu−N distances in the square planes vary between 1.973(7) and 2.034(5) Å for Cu2 and between 1.973(7) and 2.044(5) Å for Cu4, while the apical distances are longer (Cu2−N9 =

(14) Karlin, K. D.; Hayes, J. C.; Gultneh, Y.; Cruse, R. W.; McKown, J. W.; Hutchinson, J. P.; Zubieta, J. *J. Am. Chem. Soc.* **1984**, *106*, 2121−2128.

(15) Holz, R. C.; Bradshaw, J. M.; Bennett, B. *Inorg. Chem.* **1998**, *37*, 1219−1225.

(16) Holz, R. C.; Brink, J. M.; Gobena, F. T.; O'Connor, C. J. *Inorg. Chem.* **1994**, *33*, 6086−6092.

(17) Berends, H. P.; Stephan, D. W. *Inorg. Chem.* **1987**, *26*, 749−754.

(18) Oberhausen, K. J.; Richardson, J. F.; Buchanan, R. M.; McCusker, J. K.; Hendrickson, D. N.; Latour, J. M. *Inorg. Chem.* **1991**, *30*, 1357−1365.

(19) Nishida, Y.; Shimo, H.; Maehara, H.; Kida, S. *J. Chem. Soc., Dalton Trans.* **1985**, 1945−1951.

(20) Belle, C.; Gautier-Luneau, I.; Gellon, G.; Pierre, J. L.; Morgenstern-Badarau, I.; Saint-Aman, E. *J. Chem. Soc., Dalton Trans.* **1997**, 3543−3546.

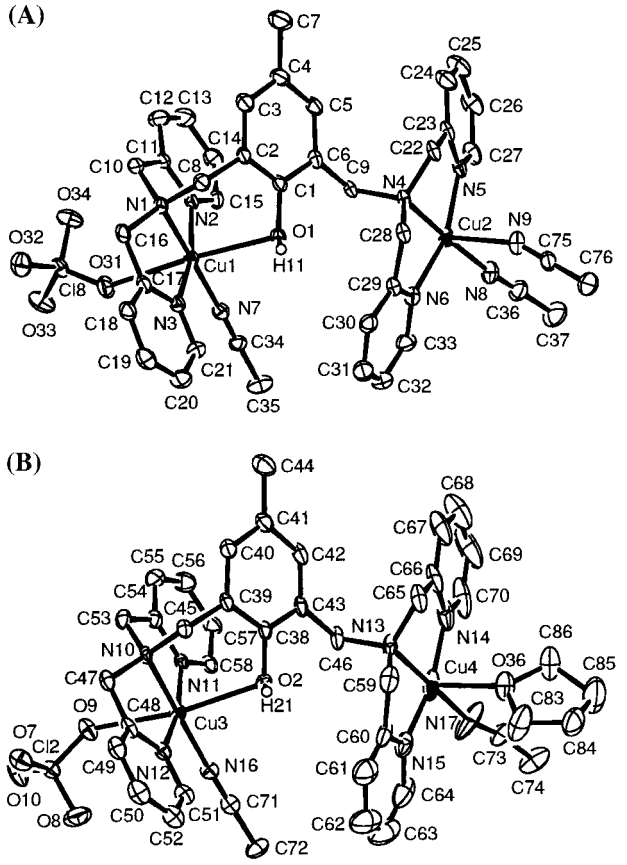

Figure 3. ORTEP plots of the two crystallographically independent units $[Cu_2(C_{33}H_{34}ON_6)(CH_3CN)_3(ClO4)]^{3+}$ (A) and $[Cu_2(C_{33}H_{34}ON_6)(CH_3CN)_2(C_4H_8O)(ClO4)]^{3+}$ (B) in complex **3**. Hydrogens are omitted for clarity. Ellipsoids are drawn at the 30% probability level.

2.355(6) Å and Cu4−O36 = 2.353(5) Å). The absence of single-atom bridges results in long intermetallic distances [(Cu1···Cu2 = 6.939(1) Å, Cu3···Cu4 = 6.923(1) Å].

Magnetic Measurements. The magnetization properties of the three complexes have been studied to evaluate the magnetic interactions between the two copper atoms. Figure 4 illustrates the temperature dependence of the product of the molar susceptibility and temperature for compounds **1** and **2**. The data for **1** show a continuous decrease of the χT product when the temperature is lowered to reach a plateau at ~0.05 cm^3 K mol^{-1}. Such behavior is characteristic of an antiferromagnetically coupled copper pair. The height of the plateau at low temperatures shows the presence of Curie behaved impurities. Indeed EPR examination reveals a contamination of the sample by ca. 4% of compound **2** and by ca. 3% of mononuclear copper(II) species. The following equations, based on the Hamiltonian H, were used to fit the magnetic data:

$$H = -2J\hat{S}_1 \cdot \hat{S}_2 + \beta\vec{H}\cdot\tilde{g}\cdot\hat{S}$$

$$\chi T = (1-p-q)\frac{3g^2}{4}\frac{1}{3+\exp\frac{-2J}{kT}} + (2p+q)\left(\frac{2.19}{2}\right)^2\frac{0.375}{1-\frac{\theta}{T}} + (\mathrm{TIP})(T)$$

The first term represents the contribution of the coupled pair with its g factor and its exchange interaction (J). The second term represents the contributions of **2** (molar fraction p) and of mononuclear copper (molar fraction q). The Weiss constant (θ) was introduced to correct the mononuclear contribution from weak additional interactions, notably those introduced by **2**. The third term represents the contribution of the temperature-independent paramagnetism (TIP). After several trials the percentage p of compound **2**, the g factor, and the Weiss constant θ were estimated to be 6%, 2.12, and − 0.8 K, respectively, and fixed in the subsequent calculations to avoid overparametrization of the system and correlations between the parameters. The parameters adjusted were the exchange coupling (J) of **1**, the percentage of mononuclear copper (q), and the TIP. The best least-squares fit reproduced in Figure 4 was obtained in the valid temperature domain of the above equation with the following parameters: $J = -112(2)$ cm^{-1}, $q = 0.046(5)$, TIP = 92×10^{-6} cm^3 mol^{-1}. The χT vs T curve shown for **2** in Figure 4 reveals that the two copper ions are essentially

Table 3: Selected Distances (Å) and Bonds Angles (deg) for **3**

Cu1	Cu2	6.939(1)	Cu3	Cu4	6.923(1)
Cu1	N2	1.983(5)	Cu3	N11	1.971(5)
Cu1	N7	1.998(5)	Cu3	N12	1.982(5)
Cu1	N3	2.003(5)	Cu3	N16	2.009(5)
Cu1	N1	2.022(5)	Cu3	N10	2.033(4)
Cu1	O1	2.432(4)	Cu3	O2	2.458(4)
Cu1	O31	2.512(4)	Cu3	O9	2.559(4)
Cu2	N6	1.981(5)	Cu4	N15	1.973(7)
Cu2	N5	1.985(5)	Cu4	N17	1.990(6)
Cu2	N8	2.003(6)	Cu4	N14	1.998(7)
Cu2	N4	2.034(5)	Cu4	N13	2.044(5)
Cu2	N9	2.355(6)	Cu4	O36	2.353(5)

N2	Cu1	O1	90.2(2)	N16	Cu3	O9	93.8(2)
N2	Cu1	O31	89.2(2)	N11	Cu3	N12	165.9(2)
N7	Cu1	N3	96.1(2)	N11	Cu3	N16	98.5(2)
N7	Cu1	N1	178.7(2)	N11	Cu3	N10	83.6(2)
N7	Cu1	O1	88.1(2)	N11	Cu3	O2	85.9(2)
N7	Cu1	O31	85.1(2)	N11	Cu3	O9	83.2(2)
N3	Cu1	N1	82.7(2)	N12	Cu3	N16	95.3(2)
N3	Cu1	O1	95.1(2)	N12	Cu3	N10	82.6(2)
N3	Cu1	O31	87.2(2)	N12	Cu3	O2	97.1(2)
N1	Cu1	O1	91.9(2)	N12	Cu3	O9	93.2(2)
N1	Cu1	O31	94.9(2)	N16	Cu3	N10	177.7(2)
O1	Cu1	O31	173.1(2)	N16	Cu3	O2	89.1(2)
N6	Cu2	N5	161.7(2)	N17	Cu4	O36	90.4(2)
N6	Cu2	N8	99.8(2)	N13	Cu4	O36	92.0(2)
N6	Cu2	N4	82.0(2)	N14	Cu4	O36	93.1(2)
N6	Cu2	N9	91.6(2)	N14	Cu4	N13	82.6(2)
N4	Cu2	N9	92.3(2)	N15	Cu4	N17	98.8(3)
N5	Cu2	N8	96.2(2)	N15	Cu4	N14	164.9(2)
N5	Cu2	N4	82.3(2)	N15	Cu4	N13	82.5(2)
N5	Cu2	N9	98.3(2)	N15	Cu4	O36	89.7(2)
N8	Cu2	N4	177.7(2)	N17	Cu4	N14	96.0(3)
N8	Cu2	N9	86.2(2)	N17	Cu4	N13	177.3(3)

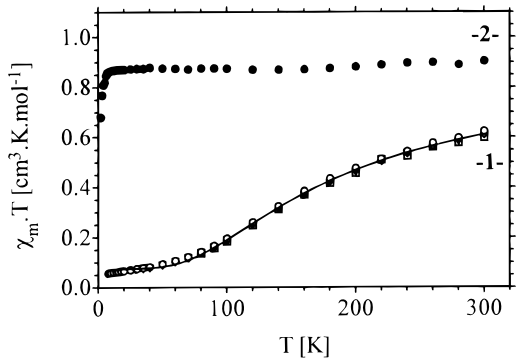

Figure 4. Temperature dependence of the product of the temperature and the molar susceptibility for complex **1** at 0.5 T (○), 1 T (◇), 2.5 T (▽), and 5 T (□) with the best least-squares fit (solid line) and complex **2** at 2.5 T (●).

uncoupled. The magnetic data were then analyzed using the Brillouin curve (see Supporting Information, Figure S1), which confirmed that **2** behaves like a normal paramagnet and that the small decrease of the χT curve at low temperature is not due to intermolecular interactions but rather to saturation effects. Fitting the Brillouin curve to the experimental data gave a spin value $S = 0.49(1)$ and a factor $g = 2.18(1)$. This behavior indicates that no magnetic interaction detectable by magnetization exists between the two copper ions. Compound **3** behaves essentially like **2** and was analyzed in the same way (see Supporting Information). A spin value $S = 0.48(1)$ and a factor $g = 2.13(2)$ were obtained from fitting the Brillouin curve to experimental data.

UV−Visible Spectroscopy. a. Complex 1. The same spectra are observed in acetonitrile or in water solutions. The shoulder observed at 410 nm ($\epsilon = 480$) corresponds to a LMCT transition between the bridging phenoxo and copper ions. Similar UV−visible features have been previously observed for several related (μ-phenoxo) dicopper(II) complexes.[4] The band observed at 785 nm ($\epsilon = 280$) is characteristic of Cu(II) d−d transitions. The position of this band suggests a trigonal bipyramidal coordination.[21] In methanolic solution, the LMCT band is shifted up to 450 nm ($\epsilon = 730$) and the d−d band appears at 770 nm ($\epsilon = 360$). This probably arises from the formation of the methoxo-bridged complex. Urbach et al.[11d] have claimed that the μ-hydroxo and the μ-methoxo complexes exhibit the same spectra in aqueous solution. In fact, their UV−visible data for the μ-methoxo complex in aqueous solution are similar to the data of our μ-hydroxo complex **1**. It is therefore likely that upon solubilization in water the methoxo bridge was replaced by a hydroxide.

b. Complex 2. The spectra are recorded in H_2O, with main features at 460 nm ($\epsilon = 710$) and 700 nm ($\epsilon = 180$) corresponding to the LMCT and to the d−d transitions, respectively. The wavelength shift (compared to **1**) observed in the d−d transition reveals the change from trigonal bipyramidal to square pyramidal coordination,[21] in agreement with the solid-state structures. The wavelength shift and intensity increase observed in the phenoxo-to-copper LMCT band for **2** compared to **1**, can be assigned to the better overlap, in the less strained open structure of the diaqua complex **2**, between the phenolate donor and the half-filled copper orbital. In methanol (472 nm, $\epsilon = 644$; 801 nm, $\epsilon = 356$) or in acetonitrile (515 nm, $\epsilon = 644$; 745 nm, $\epsilon = 600$), the changes in spectra indicate the displacement of H_2O ligand by methanol and acetonitrile, respectively.

c. Complex 3. Important changes are observed with the solvent. The d−d transition is shifted from 610 nm ($\epsilon = 266$) in acetonitrile to 695 nm ($\epsilon = 177$) in water. Moreover, a band attributated to the phenoxo-to-copper LMCT transition 460 nm ($\epsilon = 650$) is observed in water but not in acetonitrile. Therefore, the spectrum recorded in acetonitrile reveals the absence of the phenoxo bridge and is characteristic of a square planar coordination of the copper(II) centers, in accordance with the solid-state structure. In water solution, on the other hand, the phenoxo bridge is probably formed with a tetragonal coordination around the copper, giving the same spectrum as that for **2**.

EPR Spectroscopy at 100 K. a. Complex 1. The complex is EPR-silent in accordance with the strong coupling between the two copper atoms (Figure 12 at pH = 6.6). This observation is consistent with a doubly bridged structure and the short copper−copper distance evidenced in the solid state.

(21) Duggan, M.; Ray, N.; Hathaway, B. *J. Chem. Soc., Dalton Trans.* **1980**, 1342−1348.

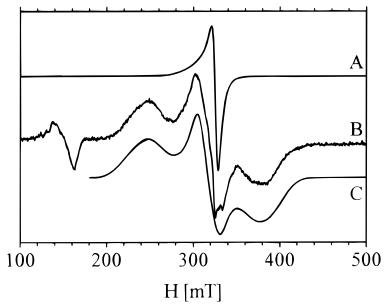

Figure 5. EPR spectrum at 100 K of **2**: (A) as a polycrystalline sample (3 mg), at microwave frequency of 9.4190 GHz, modulation amplitude of 2 mT; (B) a frozen solution of H_2O/DMSO (1:1 v/v, 3 mM), at microwave frequency of 9.4103 GHz, modulation amplitude of 2 mT; (C) simulation of (B) with $g_1 = 2.23$ (18 mT), $g_2 = 2.11$ (6.5 mT), $g_3 = 2.09$ (16 mT), $|D| = 0.076$ cm^{-1}, and $E/D = 0.27$. Both spectra were recorded with microwave power of 20 mW, modulation frequency of 100 kHz, one scan for 167 s.

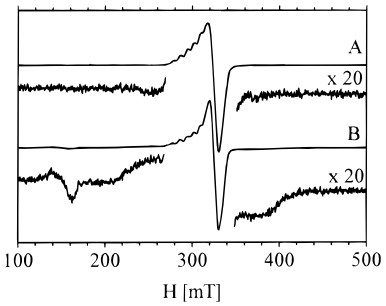

Figure 6. EPR spectrum at 100 K of **3**: (A) in CH_3CN/DMSO (3 mM), at microwave frequency of 9.4114 GHz; (B) in H_2O/DMSO (3 mM), at microwave frequency of 9.4074 GHz. Both spectra were recorded with microwave power of 20 mW, modulation frequency of 100 kHz, modulation amplitude of 2 mT, one scan for 167 s.

b. Complex 2. The spectra recorded at 100 K for a polycrystalline sample and in a frozen solution of H_2O/DMSO (1:1 v/v) are shown in Figure 5. The X-band EPR spectrum of a powdered sample of **2** at 100 K displays a signal shape similar to the spectrum of **3** (Figure 6A), with $g_\perp \approx 2.07$ (Figure 5A). A $g_\parallel$ value larger than the $g_\perp$ value is consistent with a tetragonally elongated square pyramid geometry around copper(II), in agreement with the X-ray structure. This signal can be attributed to two uncoupled or weakly coupled copper(II) ions. The EPR spectrum of **2** in frozen solution (H_2O (pH = 3)/DMSO, 1/1) suggests a change in copper coordination geometry (Figure 5B). The spectrum reveals a $\Delta M_s = \pm 2$ transition at 160 mT and a broad $\Delta M_s = \pm 1$ signal from 200 to 440 mT. Similar features were observed for **2** in CH_3CN/DMSO (1/1) with two sets of signals centered at roughly $g = 4.3$ and $g = 2$. The simulation of spectrum B shown in Figure 5C was obtained considering two coupled copper(II) ions with zero-field splitting. The simulation parameters were $g_1 = 2.23$, $g_2 = 2.11$, $g_3 = 2.09$, $|D| = 0.076$ cm^{-1}, and $E/D = 0.27$. An E/D fraction close to $^1/_3$ indicates a rhombic distortion.

c. Complex 3 in 1:1 v/v CH_3CN/DMSO. The spectrum is shown in Figure 6A. No $\Delta M_s = \pm 2$ transitions are observed. The spectrum exhibits a resolved hyperfine structure in the $g_\parallel$ region with six discernible lines with an average splitting of 7.8 mT. These features could be due to a weak exchange interaction between the two copper(II) ions. Seven hyperfine lines would occur in the $g_\parallel$ region, the seventh line overlapping the $g_\perp$ region.[22−24] Nevertheless, a detailed saturation and temperature study of the line shape of the $g_\parallel$ region shows two slightly different behaviors. Hyperfine lines at 280, 294, 310,

Table 4: Electrochemical Data[a] for **1** and **2** in CH_3CN or Aqueous Electrolyte

	in CH_3CN,[b] V	in H_2O,[c] V
1	0.75, −0.94, −1.24[d]	0.72V,[d] −0.27, *e*
2	0.65, −0.33, −0.86	0.82, −0.17, −0.46[d]

[a] $E_{1/2}$ or E_{pc} (see foonote *d*) determined by CV, $\upsilon = 0.1$ V s^{-1}. [b] V vs 10 mM $Ag/AgNO_3$ + 0.1 M TBAP + CH_3CN. [c] V vs SCE. [d] Irreversible. [e] Not observable in the accessible potential range.

and 325 mT are more easily saturated than hyperfine lines at 286, 302, and 317 mT (for example, at 13 K, between 0.2 and 12.6 mW). The presence of two sets of hyperfine lines suggests the overlap of two signals of uncoupled copper(II) ions. Two values are measured for $g_{||}$ (2.22 with $a_{||} \approx 160 \times 10^{-4}$ cm^{-1}, and 2.28 with $a_{||} \approx 165 \times 10^{-4}$ cm^{-1}) and one for $g_{\perp}$ (2.07). This result is in accordance with the solid-state structure (intermetallic distance ≈ 7 Å).

d. Complex 3 in 1:1 v/v H_2O/DMSO. The spectrum is shown in Figure 6B. A $\Delta M_s = \pm 2$ transition at 160 mT and shoulders at 240 and 380 mT are observed, revealing the presence of complex **2** (see above) in addition to complex **3**. These observations corroborate the conclusions from UV−visible data.

^{1}H NMR Studies. The ^{1}H NMR spectrum of **1** in CD_3CN at 60 °C has been reported by Holz et al.[11a−c,e] The signals had been assigned by inspection of their peak areas and from T_1 values. In D_2O, **1** displays a qualitatively similar spectrum with relatively sharp and well-defined resonances (0−180 ppm chemical shift range) except for the absence of the μ-hydroxo proton exchanged with D_2O. **2** in D_2O at room temperature exhibits the spectrum depicted in Figure 13 with broad signals in the paramagnetic region. The assignments of the remaining signals of **2** were deduced from **1** and from the progressive pH-driven changes from **1** to **2** in ^{1}H NMR spectra (the chemical shift assignments for **1** and **2** are in Table S1 of the Supporting Information). No spectrum can be obtained in CD_3CN at 298 K for **3**. In D_2O, the same spectrum as observed for **2** is obtained: **3** is irreversibily transformed into **2** upon dissolution in water. All the observations are in accordance with the conclusions from the other spectroscopies.

Electrochemical Results. The electrochemical behavior of **1** and **2** has been studied in CH_3CN and aqueous electrolytes by cyclic voltammetry (CV) and rotating disk electrode (RDE) voltammetry. All the results are summarized in Table 4. When scanning toward the negative region of potentials, the CV curve recorded in a CH_3CN electrolytic solution of **1** is characterized by two successive one-electron electrochemical signals (Figure 7). The first one at $E_{1/2} = -0.94$ V ($\Delta E_p = 0.10$ V, $\upsilon = 0.1$ V s^{-1}) appears reversible (Figure 7B) and corresponds to the complexed $Cu_2^{II,II}/Cu_2^{II,I}$ redox couple. The second one corresponding to the formation of the $Cu_2^{I,I}$ species at $E_{pc} = -1.24$ V is fully irreversible, suggesting a fast decomposition of the $Cu_2^{I,I}$ form of **1**. As previously described,[25] OH^- bridges have a poor ability to bind Cu^I centers and tend to dissociate upon electrogenerated reduction. The anodic part of the CV curve (Figure 7B) shows one pair of peaks, revealing the reversible one-electron oxidation of **1** at $E_{1/2} = 0.75$ V ($\Delta E_p = 0.10$ V, $\upsilon = 0.1$ V s^{-1}). Further oxidation occurring at $E_{pa} = 1.32$ V is fully irreversible. The voltammogram recorded at the RDE

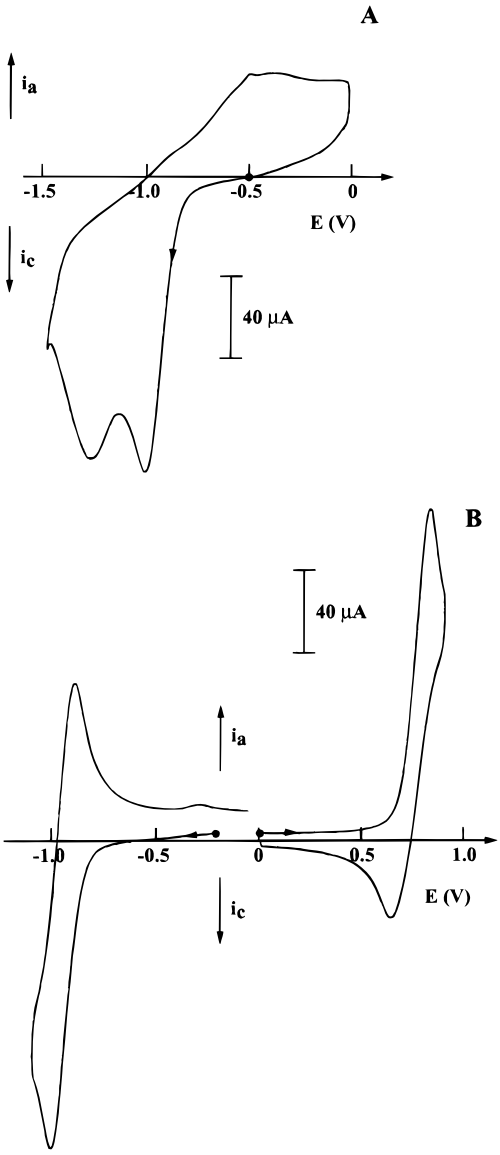

Figure 7. Cyclic voltammograms for a 4 mM solution of complex **1** in CH_3CN + 0.1 M TBAP at a vitreous carbon disk (5 mm diameter), $\upsilon = 0.1$ V s^{-1}, V vs 10 mM $Ag/AgNO_3$ + CH_3CN + 0.1 M TBAP: (A) scan between 0 and −1.5 V starting at −0.5 V; (B) scans between 0 and 0.9 V and then between −0.2 and −1.1 V.

displays a well-behaved anodic wave at $E_{1/2} = 0.75$ V. The cathodic wave corresponding to the first reduction of **1** shows a continuous decrease of the limiting current characteristic of adsorption phenomena. This precludes any observation of the second cathodic wave. In aqueous medium (pH = 8) containing **1**, the CV curve (Figure 8) displays in the negative region of potentials a weakly reversible system at $E_{1/2} = -0.27$ V ($\Delta E_p = 0.10$ V, $\upsilon = 0.1$ V s^{-1}). Further reduction is not observable in the accessible potential range in aqueous medium. Oxidation of **1** appears as a shoulder ($E_{pa} = 0.72$ V) on the solvent oxidation barrier. The CV curve recorded in a CH_3CN solution of **2** (acetonitrile derivatives, see UV−vis discussion) (Figure 9A) displays in the negative region of potentials two cathodic electrochemical signals. The first one appearing at $E_{1/2} = -0.33$ V ($\Delta E_p = 0.19$ V, $\upsilon = 0.1$ V s^{-1}) is weakly reversible and corresponds to the complexed $Cu_2^{II,II}/Cu_2^{II,I}$ redox couple. The second one leading to the $Cu_2^{I,I}$ form of **2** is also weakly reversible at $E_{1/2} = -0.86$ V ($\Delta E_p = 0.15$ V, $\upsilon = 0.1$ V s^{-1}). In addition, on the reverse scan, an extra sharp anodic peak at

(22) Mandal, S. K.; Thompson, L. K.; Newlands, M. J.; Gabe, E. J.; Lee, F. L. *Inorg. Chem.* **1990**, *29*, 3556−3561.
(23) Tandon, S. S.; Thompson, L. K.; Bridson, J. N.; Dewan, J. C. *Inorg. Chem.* **1994**, *33*, 54−61.
(24) Monzani, E.; Quinti, L.; Perotti, A.; Casella, L.; Gullotti, M.; Randaccio, L.; Geremia, S.; Nardin, G.; Faleschini, P.; Tabbi, G. *Inorg. Chem.* **1998**, *37*, 553−562.

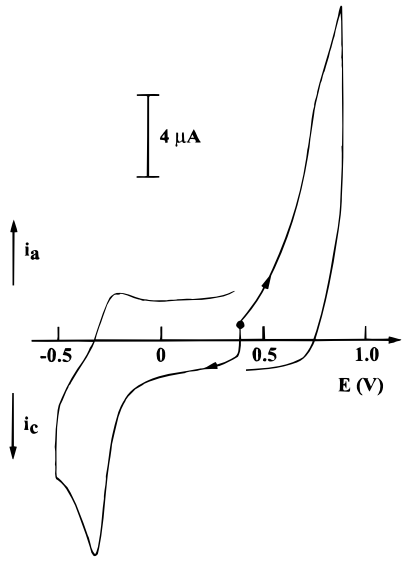

Figure 8. Cyclic voltammograms for a 0.4 mM solution of complex **1** in H_2O + 0.1 M $NaClO_4$ (tris-buffered at pH = 8) at a vitreous carbon disk (5 mm diameter), $\upsilon = 0.1$ V s^{-1}, V vs SCE, scans between 0.4 and 0.9 V and then between 0.4 and −0, 50 V.

$E_{pa} = -0.52$ V is seen on the CV curve. This is characteristic of a redissolution process, suggesting that the two-electron reduction of **2** is accompanied by its partial decomposition and by a further reduction in the same range of potentials, leading to a deposit of Cu^0 onto the electrode surface that is redissolved at −0.52 V. As for **1**, the anodic part of the CV curve exhibits a reversible pair of peaks at $E_{1/2} = 0.65$ V ($\Delta E_p = 0.09$ V, $\upsilon = 0.1$ V s^{-1}) corresponding to the one-electron oxidation of **2**. The voltammogram at the RDE (Figure 9B,C) displays one well-behaved anodic wave at $E_{1/2} = 0.68$ V (Figure 9B) when three cathodic waves (Figure 9C) are seen. The first one at $E_{1/2} = -0.38$ V of about the same intensity as that of the anodic wave corresponds to the formation of the mixed valent $Cu_2^{II,I}$ form of **2**. The second one at $E_{1/2} = -0.63$ V presents a smaller height and is followed by a third cathodic wave at $E_{1/2} = -0.85$ V. The sum of the heights of the second and the third cathodic waves is close to that found for the first cathodic wave, indicating that the reduction of the $Cu_2^{II,I}$ form of **2** is accompanied by the formation of two species at equilibrium. The formation of two reduced species has already been observed for comparable systems[25] and resulted from changes in the coordination sphere upon a change of the oxidation state. In an aqueous medium, the electrochemical behavior of **2** studied by CV (Figure 10) is characterized by two successive cathodic electrochemical systems. The first one, which is reversible, appears at $E_{1/2} = -0.17$ V ($\Delta E_p = 0.06$ V, $\upsilon = 0.1$ V s^{-1}) and leads to the mixed valent $Cu_2^{II,I}$ species. Further reduction at $E_{pc} = -0.46$ V is irreversible and corresponds to the formation of the $Cu_2^{I,I}$ species followed by the deposition of Cu^0 onto the electrode surface as judged by the appearance on the reverse scan of a sharp anodic peak at $E_{pa} = -0.06$ V corresponding to the redissolution of Cu^0. On the anodic part of the CV curve, the quasi-reversible oxidation of **2** is seen at $E_{1/2} = 0.82$ V ($\Delta E_p = 0.24$ V, $\upsilon = 0.1$ V s^{-1}) at the threshold of the solvent oxidation.

pH-Driven Interconversions in H_2O. UV−visible titration (monitoring of the LMCT band) of **1** with perchloric acid (3.8 < pH < 6.6) leads quantitatively to **2**. An isosbestic point is observed at 392 nm, indicating the presence of only two absorbing species. An intermediate species such as an aquahydroxodicopper(II) complex is not detected. The reaction is fully reversible by addition of sodium hydroxide to the solution of **2** (Figure 11). A plot of the absorbance vs pH indicates that the

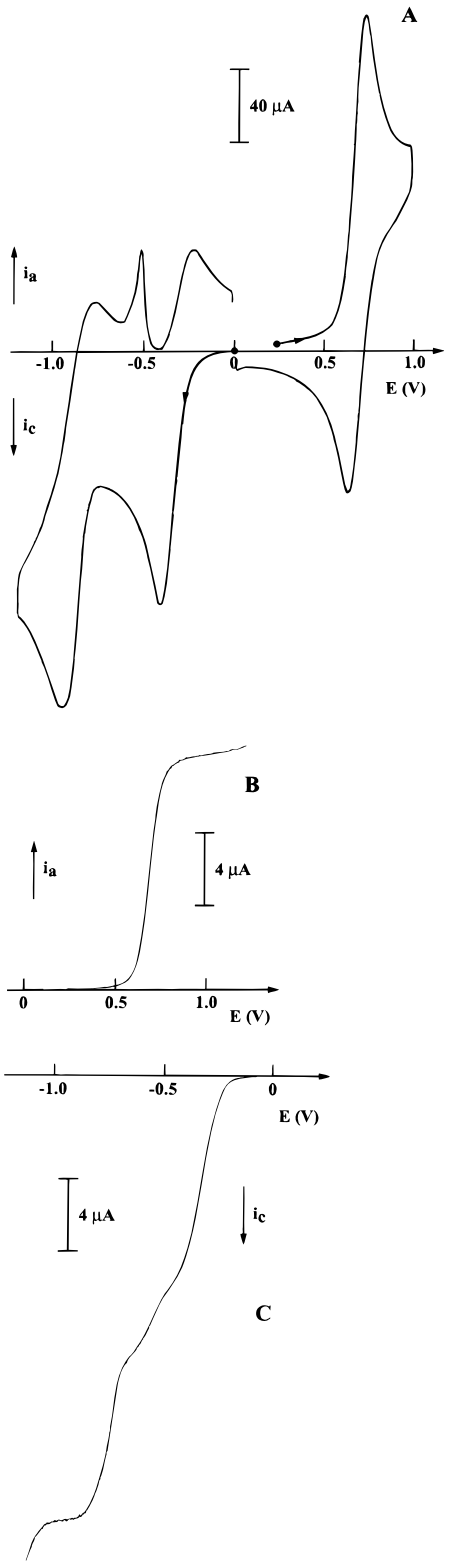

Figure 9. Voltammograms for a solution of complex **2** in CH_3CN + 0.1 M TBAP at a vitreous carbon disk (5 mm (A) or 3 mm (B, C) diameter), V vs 10 mM $Ag/AgNO_3$ + CH_3CN + 0.1 M TBAP: (A) CV curve in a 4 mM solution at $\upsilon = 0.1$ V s^{-1} with scans between 0.2 and 1.0 V and then between 0 and −1.2 V; (B) voltammogram in a 2 mM solution at the RDE (600 rpm), anodic part; (C) same as (B), cathodic part.

(25) Reim, J.; Krebs, B. *J. Chem. Soc., Dalton Trans.* **1997**, 3793−3804.

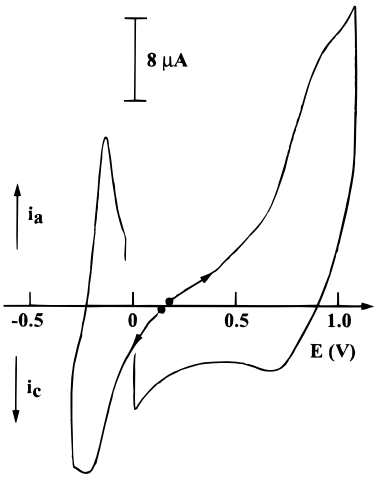

Figure 10. Cyclic voltammograms in 0.8 mM solution of complex **2** in H_2O + 0.1 M $NaClO_4$ at a vitreous carbon disk (5 mm diameter), v = 0.1 V s^{-1}, V vs SCE, scans between 0.2 and 1.0 V and then between 0.2 and −0.25 V.

deprotonation process has an apparent pK_1 of 4.95 (±0.05) to 25 °C (according to the method of Schwarzenbach).[26] Another species (complex **4**) is reversibly formed in strong basic medium (pK_2 = 12.0). **4** (which could not be obtained in the solid state) gives UV−visible main spectral features at 420 nm (ϵ = 670) attributed to the LMCT phenoxo-to-metal transition and 695 nm (ϵ = 480) attributed to the Cu(II) d−d transition. The EPR spectrum of **4** in 1:1 v/v H_2O/DMSO at 100 K (Figure 12 at pH = 12.1) is similar to complex **2** and reveals $\Delta M_s = \pm 1$ transitions from 200 to 420 mT and $\Delta M_s = \pm 2$ transitions at 150 mT. This spectrum is typical of an S = 1 state of two coupled copper(II) ions. A dihydroxostructure (depicted in Figure 11) is proposed for **4** (see discussion part). Strong acidification (pH < 3) of **2** leads to the release of free copper ions. The equilibrium between **1**, **2**, and **4** has been also studied by EPR spectroscopy in 1:1 v/v H_2O/DMSO at 100 K (Figure 12) and by ^{1}H NMR in D_2O (DMSO) at 298 K (Figure 13). Upon addition of CF_3CO_2D or NaOD (1 M), large changes were observed in the ^{1}H spectrum of **1** in D_2O. Decreasing the pH from 6.6 to 4.2 leads to a decrease in the intensity of the observed ^{1}H NMR signals, which were broader and slightly shifted. Near pH 4 some signals disappeared, and the original spectrum of **2** was obtained. From pH 6.6 to 12.1, a similar evolution occurred and a new spectrum was observed and attributed to **4**. The spectrum of **1** was fully restored when the pH was lowered to 6.6. Since the hyperfine shifted ^{1}H NMR signals obtained for dicopper(II) centers are a function of spin coupling between the two Cu(II) ions, these data suggest that the two Cu(II) ions in **4** become less uncoupled than **1** in a similar trend as for **2** (see magnetism paragraph). The pH dependence of the methyl protons chemical shift (δ) can be quantitatively treated using a Schwarzenbach-type equation

$$\delta = \delta_1 + K_1(\delta_2 - \delta)/[H^+]$$

where K_1 is the ionization constant (acidic medium), δ_1, δ_2, and δ the observed chemicals shifts for species **1**, **2**, and the mixture of the two in fast exchange. A pK_1 value can be obtained (4.9) that is in good agreement with the value obtained from UV−visible titration. Determination of pK_2 by a similar treatment affords a value of 13.1.

(26) Schwarzenbach, G.; Schwarzenbach, K. *Helv. Chim. Acta* **1963**, *46*, 1390−1400.

Discussion

Magnetic Studies. The two phenoxo-bridged complexes **1** and **2** in the solid state behave differently because **2** is essentially uncoupled while **1** exhibits a moderate antiferromagnetic coupling. The crystallographic study has revealed that the two copper atoms of **2** are in square pyramidal environments with the phenoxo oxygen occupying both apical positions. The $d_{x^2-y^2}$ based magnetic orbitals are located in the N3O planes of each copper atoms, and therefore, they have negligible overlap, which explains the lack of exchange interaction. Changes in the coordination geometry of the copper atoms may explain the increase of exchange coupling, allowing the observation of an S = 1 EPR spectrum. The situation of **1** is less straightforward. Indeed, examination of the literature reveals that the exchange coupling found for the 17 (μ-hydroxo)(μ-phenoxo) complexes both structurally and magnetically characterized span a ∼900 cm^{-1} range.[13,14,27−29] As expected both on theoretical and experimental grounds, the following general trend is observed: the wider the Cu−O(H)-Cu angle, the stronger the antiferromagnetic coupling. Nevertheless, significant differences exist for compounds with Cu−O(H)−Cu angles of similar magnitudes. The reasons for the latter effect may be found in the geometrical distortions, which affect the copper coordination spheres, the geometries of the bridges, and the planarity of the Cu2O2 core. It is worth noting that the value of the exchange interaction obtained in the present study, $-2J$ = 224 cm^{-1}, is close to that obtained earlier by Holz,[11b,c] $-2J$ = 187 cm^{-1}, which is consistent with the small structural variation between the two forms of the compound. However, these two values are significantly smaller ($\Delta J \approx 300$ cm^{-1}) than those estimated for the two complexes with similar Cu−O(H)−Cu angles,[28,29] and this reflects substantial differences in the copper coordination spheres. In the latter complexes the copper atoms possess tetragonal symmetries, square pyramidal or elongated octahedral, with both the hydroxo and the phenoxo bridges in the tetragonal plane. The $d_{x^2-y^2}$ copper-based magnetic orbitals point toward both bridging oxygens. On the other hand, for **1** and Holz's compound, the copper atoms are in trigonal bipyramidal environments with the hydroxo oxygen in the axial positions. The magnetic orbitals are d_{z^2}, which point toward the hydroxo bridge, and therefore, a negligible contribution of the second bridge is expected in line with the reduced exchange interaction.

Electrochemical Data. By comparing the results obtained in CH_3CN and aqueous electrolyte, one can conclude that for **2**, the gap between the oxidation and the first reduction processes is independent of the solvent and is close to 0.99 V. In addition, referring the corresponding $E_{1/2}$ obtained in CH_3CN to the SCE reference electrode (−0.30 V vs 10 mM $Ag/AgNO_3$ + 0.1 M TBAP + CH_3CN), i.e., $E_{1/2}$ = 0.95 V vs SCE and −0.03 V vs SCE for the oxidation and the first reduction of **2** in CH_3CN, respectively, one can estimate the solvent effect on the electrochemical properties of **2**. A positive shift close to 0.13 V is determined for both redox potentials from the aqueous electrolyte to the CH_3CN medium. This is consistent in that for

(27) (a) Benzekri, A.; Dubourdeaux, P.; Latour, J. M.; Laugier, J.; Rey, P. *Inorg. Chem.* **1988**, *27*, 3710−3716 and references therein. (b) Uozumi, S.; Ohba, M.; Okawa, H.; Fenton, D. E. *Chem. Lett.* **1997**, 673−674. (c) Ghosh, D.; Mukherjee, R. *Inorg. Chem.* **1998**, *37*, 6597−6605. (d) Asokan, A.; Varghese, B.; Manoharan, P. T. *Inorg. Chem.* **1999**, *38*, 4393−4399.

(28) O'Connor, C. J.; Firmin, D.; Pant, A. K.; Babu, B. R.; Stevens, E. D. *Inorg. Chem.* **1986**, *25*, 2300−2307.

(29) (a) Gagné, R. R.; McCool, M. W.; Marsh, R. E. *Acta Crystallogr., Sect. B* **1980**, *B36*, 2420−2422. (b) Grzybowski, J. J.; Merrell, P. H.; Urbach, F. L. *Inorg. Chem.* **1978**, *17*, 3078−3082.

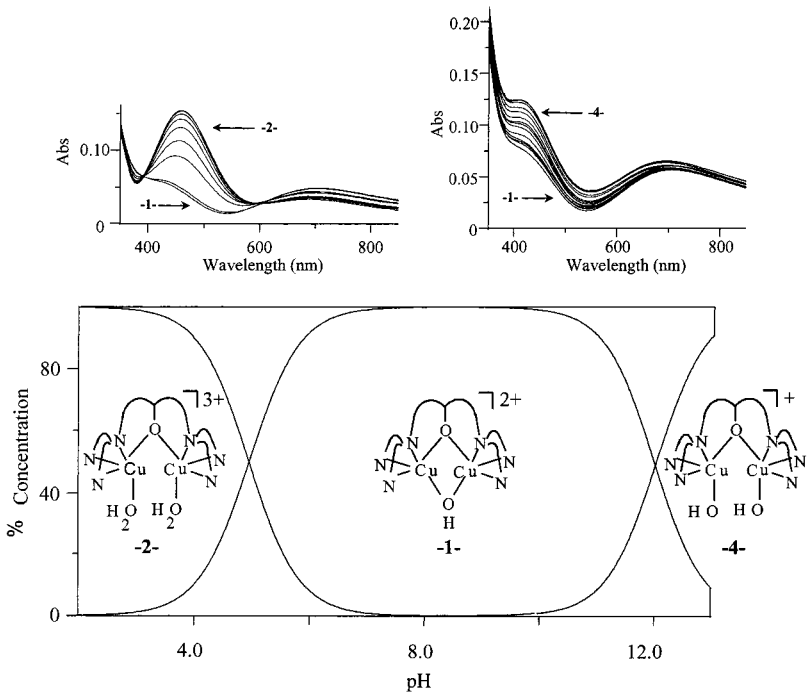

Figure 11. UV−visible titration of **1** (sodium hydroxide and perchloric acid in aqueous solution) and species distribution curves as a function of pH.

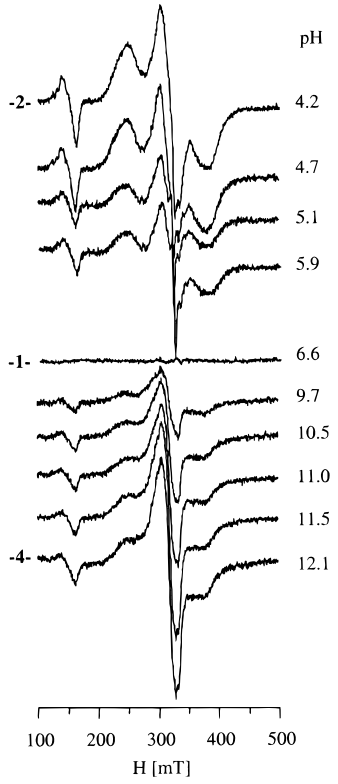

Figure 12. pH-driven changes of **1** in EPR studies at 100 K, in H_2O/DMSO (1:1 v/v, 3 mM). Microwave frequencies are 9.407(3) GHz. Both spectra were recorded with a microwave power of 20 mW, modulation frequency of 100 kHz, modulation amplitude of 0.2 mT, and one scan for 167 s. The pH was adjusted with $HClO_4$ or NaOH (1 M).

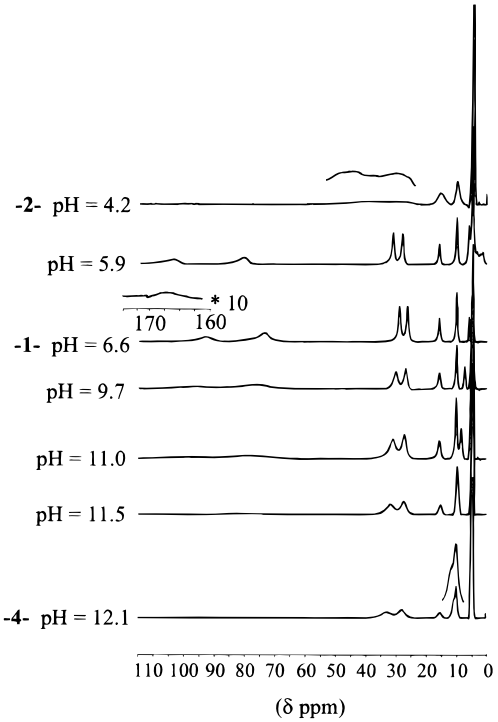

Figure 13. pH-driven changes of **1** in ^1H NMR studies at 25 °C, in D_2O with a drop of DMSO as solvent. The pH was adjusted with CF_3CO_2D and NaOD (1 M).

H_2O to CH_3CN electrolyte, **2** solely undergoes a change in the solvent coordination. The same conclusions cannot be drawn for **1**; the gap between oxidation and the first reduction is dependent on the solvent (1.69 V in CH_3CN and 0.99 V in H_2O), and compared to the CH_3CN electrolyte, **1** appears easier to be oxidized and reduced in aqueous medium by 0.33 and 0.37 V, respectively. On the other hand, from data shown in Table 4, compared to the electrochemical stability of **2**, **1** is stabilized by 0.61 and 0.90 V toward its reduction in CH_3CN and H_2O electrolytes, respectively.

pH-Driven Interconversion. The pH-driven interconversion processes are depicted in Figure 14. The species **1** and **2** have been fully characterized, while **4** is a proposed structure in

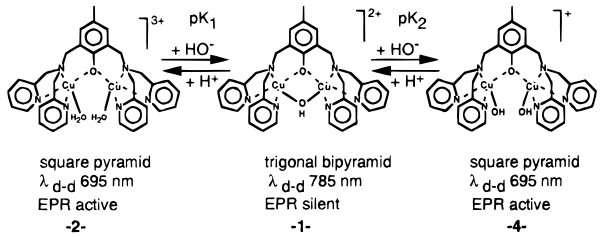

Figure 14. pH-driven interconversions between **1**, **2**, and **4**.

accordance with the experimental results in solution. Titration of **1** with sodium hydroxide is accompanied by a shift in the LMCT band (from 410 to 420 nm) and in the Cu(II) d−d band (from 785 to 695 nm) with a concomitant increase in the molar absorptivities. The wavelength of the Cu(II) d−d band (similar to that of complex **2**) suggests a square pyramidal coordination sphere around the copper ions. For the strongly coupled complex **1**, there is no detectable EPR spectrum and several isotropically shifted ^{1}H NMR are observed. As the pH decreases, the EPR signal becomes detectable, revealing a moderate coupling between copper ions (complex **2**). A similar trend for the pH 6.6−12.1 is observed, revealing a moderate coupling between the two copper(II) ions (complex **4**). Both **2** and **4** exhibit several ^{1}H NMR signals broader than that observed with **1**. Taken together, these data confirm that the copper centers in **2** and **4** are weakly magnetically coupled, providing EPR and ^{1}H NMR spectra with similar features. The (μ-phenoxo)bis(hydroxo)-dicopper(II) structure proposed for **4** is in accordance with results obtained by several methods (UV−vis, EPR, ^{1}H NMR titrations) that lead to similar conclusions. It is emphasized that a small pH change can induce noticeable variations in the coordination spheres around the metal centers, and then in the spectroscopic properties and in the reactivities (see below).

Catechol Oxidase Activities. Catechol oxidases are type III copper proteins that catalyze the oxidation of catechols to quinones [see ref 25 and references cited therein]. They are isolated in the antiferromagnetically coupled Cu(II)−Cu(II) *met* form, which involves a μ-hydroxo dicopper center with a very short Cu−Cu distance of 2.87 Å.[30−32] The catecholase activity of several dicopper complexes has been investigated, allowing correlation between activity and structural parameters.[24,25] It seemed interesting to study this activity with the complexes described in this paper, with the aim of correlating their activity (or their lack of activity) with their structural and electronic parameters related to the pH dependence described above. 3,5-Di-*tert*-butylcatechol (3,5-DTBC) has been employed as the substrate, and the activities and reaction rates have been determined by monitoring the time dependence of absorption of the quinone (3,5-DTBQ). All the complexes described above (**1**−**4**) have been studied; only **1** exhibits catecholase activity (Figure 15). Addition of a small amount of acid or base stopped the catecholase activity, which was fully restored when the pH was adjusted to 6−8, i.e., in the range where **1** is the only species present (Figure 11). These results indicate the dependence on the changes in geometry of the metal complexes for catalytic ability. The reaction rate in acetonitrile was obtained from the slope of the trace at 410 nm, and the Lineweaver−Burk treatment gave $v_{max} = 1.1 \times 10^{-6}$ M^{-1} s^{-1} and $K_M = 1.49$ mM. These values are in the range of the values observed for dicopper complexes described in the literature.[25] Because **2** is more easily reduced than **1**, the redox potential of the dicopper complexes is not decisively related to the observed activities. As observed in the structure of **1**, the metallic site is easily accessible and the short Cu−Cu distance (2.96 Å in **1** versus 4.13 in **2**) will allow a bridging catechol coordination compatible with the distance between the two *o*-diphenol oxygen atoms (a Cu−Cu distance of 3.25 Å was measured for the unique *o*-catecholate-bridged dicopper complex described in the literature).[33] It is emphasized that this distance is 2.9 Å in the enzyme, which is also a μ-hydroxo dicopper complex. Similar conclusions had been reached by Krebs.[25] Moreover, the change of coordination sphere from **1** to **2** (from trigonal bipyramid to square pyramid) increases the steric bulk around the copper atoms, preventing the catechols from approaching. The activity of the enzyme[32] is observed in the pH 5−8 range (optimum activity at pH 8), with an irreversible loss of activity below pH 4.0 and above pH 10.0. It is noted that this pH range of activity corresponds exactly to the domain existence of the μ-hydroxo complex **1** (Figure 11). Work is in progress to investigate whether this is fortuitous or reveals an intrinsic property of the μ-hydroxo dicopper(II) core.

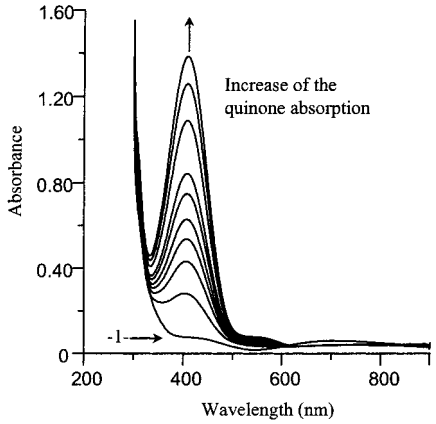

Figure 15. Time dependent growth of 3,5-DTBQ catalyzed by **1**.

Acknowledgment. The authors are grateful to Dr. Alain Deronzier for his interest in this work, to Dr. André Jeunet for his assistance in the EPR spectroscopic studies, to Fabrice Thomas for help with the p*K* determinations, and to Guy Serratrice and Serge Gambarelli for fruitful discussions.

Supporting Information Available: Listings of the molar magnetization vs $\beta H/(kT)$ for complexes **2** and **3** with the best least-squares fit; a table of ^{1}H NMR data for **1** and **2** in D_2O solution; a structure showing a different view for **1** and **2** and stereoviews for **1** and **2**; and tables of crystal data and structure refinement, positional atomic and thermal parameters, bond lengths and angles for **1**−**3**. This material is available free of charge via the Internet at http://pubs.acs.org.

IC991450Z

(30) Eicken, C.; Zippel, F.; Büldt-Karentzopoulos, K.; Krebs, B. *FEBS Lett.* **1998**, *436*, 293−299.
(31) Klabunde, T.; Eicken, C.; Sacchettini, J. C.; Krebs, B. *Nature Struct. Biol.* **1998**, *5*, 1084−1090.
(32) Rompel, A.; Fischer, H.; Meiwes, D.; Büldt-Karentzopoulos, K.; Dillinger, R.; Tuczek, F.; Witzel, H.; Krebs, B. *J. Biol. Inorg. Chem.* **1999**, *4*, 56−63.
(33) Karlin, K. D.; Gultneh, Y.; Nicholson, T.; Zubieta, J. *Inorg. Chem.* **1985**, *24*, 3725−3727.